1
2
3
4
5
6
7
8
9
10
11
12
13
14
15
16
17
18
19
20
21
22
23
24
25
26
27
28
29
30
31
32
33
34
35
36
37
38
39
40
41
42
43
44
45
46
47
48
49
50
51
52
53
54
55
56
57
58
59
60
61
62
63
64
65

A comparative analysis of site-specific response spectral amplification models

Valerio Poggi[1,2,*], Benjamin Edwards[1,3], Donat Fäh[1]

1. Swiss Seismological Service, ETH Zürich
2. Global Earthquake Model foundation (GEM), Pavia, Italy
3. University of Liverpool, United Kingdom

*Corresponding author: valerio.poggi@globalquakemodel.org
Global Earthquake Model foundation (GEM),
Via Ferrata 1, 27100 Pavia, Italy
Tel. +39 339 5994678

1

Abstract

In the framework of the Seismic Hazard Harmonization in Europe (SHARE) project, the Swiss Seismological Service (SED) has performed an evaluation of two procedures developed to produce soil amplification models for 5% damped pseudo-spectral acceleration response spectra, each using different parameters to describe the soil properties. The goal of the work presented here is to evaluate the statistical consistency of the methods, with particular regard to their applicability to engineering practice. Additionally, we compare the results with those from a methodology internally developed by the SED, which is based on spectral modeling of ground motion using the quarter-wavelength approximation to parameterize soil conditions. Soil amplification is computed with respect to reference rock condition as defined for the probabilistic seismic hazard assessment performed during the SHARE project.

For the comparison, a residual analysis was performed between the computed soil-amplification functions from the three different methodologies, over a number of selected sites spanning different soil classes and ground motion levels. The analysis of the average residuals of these functions is useful to highlight the main differences between the proposed approaches, with special regard to the impact of soil resonances and anelastic attenuation within different frequency bands.

The assessment was performed on a group of 88 selected stations of the Japanese KiKNet strong-motion network, for which complete logs of the shear-wave velocity profiles are available, in addition to a significant number of earthquake recordings. In a first step, average residuals were computed. Subsequently, amplification variability related to soil classes was investigated. The target of this second step was to perform the comparison by separately analyzing the impact of different soil and velocity classes, according to a soil-classification scheme proposed by Aristotle University of Thessaloniki (AUTH). In this paper the main results of these investigations are summarized and, when applicable, an interpretation of our findings is given.

1 - Introduction

Large earthquakes cause significant surface ground shaking. The extent of this shaking at local scales is largely controlled by the effect of geology (e.g., Aki, 1988; Faccioli, 1991). For example, the presence of loose low-velocity sediments overlying bedrock can result in significant amplification of ground motion at the surface. The increase in observed intensity can, in some cases, be equivalent to a unit in earthquake magnitude. This can mean the difference between different structural damage states or even collapse. In order to properly predict the effect of such local amplification on building and structures, an accurate modeling of soil behavior is necessary (e.g. Pitilakis, 2004). However, due to the complexity of the phenomenon, full seismic site-response evaluation requires detailed knowledge of the subsurface, which is often too expensive to be obtained over numerous sites.

To overcome this lack of information, empirical and numerical amplification models are widely used. These models are typically based on the definition of soil proxies (e.g. the average shear-wave velocity over the first 30m Vs30, geotechnical classification, etc.) and are calibrated on observed ground motion and site-specific information. The reliability of such models, however, strongly depends on the size and consistency of the input datasets, in addition to the chosen level of model-simplification related to the underlying working assumptions (e.g. one-dimensionality of the soil profile, linear vs. non-linear models). Nevertheless, progressive assimilation of new data and subsequent implementation of more sophisticated models help to reduce bias and epistemic uncertainty of the prediction. This has a direct impact on the reduction of the total uncertainty in ground motion analysis, seismic hazard and risk modeling.

Unfortunately, the available site characterization information used for developing amplification models is highly fragmented worldwide and very few attempts of harmonization have been carried out so far. There is therefore a clear need to compare existing site-specific studies. In this context, it is essential to improve the current state of art and to define new strategies for future developments (Douglas & Edwards, 2016).

3

In this study we present the results of a comparison between three different amplification models for 5% damped pseudo-spectral acceleration response spectra calibrated on a reference ground motion prediction equation (GMPE) using rock reference condition defined by Vs30 of 800m/s. The work was initiated by the SHARE project (Woessner et al., 2015), with the goal of performing a round of independent verification of the procedures proposed by Aristotle University of Thessaloniki (AUTH) and Middle East Technical University (METU) for site-specific ground motion prediction.

We extended the analysis by further comparing response spectral amplification functions with those from a methodology developed by the Swiss Seismological Service (SED). The comparison was done for 88 selected sites of the Japanese KiKNet strong-motion network (Aoi et al., 2004). Our method to estimate soil amplification is described in Poggi et al. (2012a) and is based on the use of the quarter-wavelength approximation (Joyner et al., 1981; Boore, 2003) to obtain a frequency-dependent representation of soil conditions, including the average quarter-wavelength velocity (Qwl-Vs) and quarter-wavelength impedance contrast (Qwl-IC). These proxies are then used to predict amplification factors using a parametric model calibrated against empirical amplification from direct observation and spectral modeling of a large number of earthquakes.

It has to be stressed that, when comparing average response amplification functions, the difference in the ground motion reference rock conditions has to be accounted for through adjustment to a common reference (Cotton et al., 2007). The SHARE amplification functions (from AUTH and METU) are computed for a common rock reference profile with Vs30 of 800m/s (a modification of the Boore and Joyner (1997) generic rock profile; Van Houtte et al. (2011)). However the SED model is defined for a harder rock (Poggi et al., 2011) and therefore needs an adjustment. Not accounting for the difference in the reference would lead to a systematic bias in the distribution of the amplification residuals. The SED model has therefore been adjusted using the procedure proposed by Edwards et al. (2013).

4

In the following, we summarize the main steps of the study, including a description of the input datasets (ground-motion recordings and site classification) and of the procedures necessary to adjust the SED model to the common rock reference. Finally, a discussion on the sensitivity of the results to different site classes and average velocities is provided, and the main findings discussed.

2 - Response spectral amplification functions

2.1 - AUTH

The scheme proposed by AUTH to compute response spectral amplification (Pitilakis et al., 2012) is similar to that prescribed by EUROCODE8 (EC8, European Committee for Standardization, 2004). Recipes are provided to reconstruct site-dependent design response spectra for a number of soil classes, which are classified on the basis of the travel-time average velocity down to the bedrock depth (VsZ) and of estimates of the fundamental frequency of resonance at the site (f_0). The major difference with respect to EC8 is the classification scheme, with an extended number of classes (8, as opposed to 5 in EC8), is that the AUTH approach explicitly accounts for the resonance of soft sediments sites. Although this method does not directly provide response spectral amplification functions, it is possible to derive such functions indirectly by normalizing the design response spectra of the target class with that from class "A", which in this case represents the reference rock of the computation.

2.2 - METU

METU proposed a GMPE-like approach to obtain non-linear response spectral amplification, (Sandıkkaya et al., 2013) which is based on a modification of the approach of Abrahamson and Silva (2008). Their method makes use of the average travel-time velocity over the first 30m (Vs30) and peak ground acceleration (PGA) estimates to calibrate the model coefficients and to subsequently back-reconstruct the non-linear amplification functions. For the comparison shown here, however, only low to

moderate magnitude earthquakes were used ($M_w \leq 6$); the analysis is therefore assumed to be in the range of the linear soil response only.

2.3 - SED

The SED has proposed a method to predict anelastic Fourier amplification functions from local site parameters estimated using the quarter-wavelength (Qwl) representation (Poggi et al., 2012a). The method was calibrated by directly comparing empirical amplification from parametric spectral modeling of earthquake recordings with average quarter-wavelength velocities (Qwl-Vs) and impedance contrasts (Qwl-IC) from 220 soft sediment sites of the Japanese KiKNet strong-motion network. The approach was based on procedures used by Edwards et al. (2011) and Poggi et al. (2012b) for predicting the vertical-to-horizontal spectral ratios for rock and soft sediment sites.

While this approach does not directly model amplification factors in terms of response spectra, response spectral amplification can be subsequently obtained through stochastic modeling of the target earthquake event (Boore, 2003). In practice, for each given magnitude, distance, source depth and stress-drop, a number of synthetic seismograms were generated using random vibration theory (Cartwright and Longuet-Higgins (1956), Liu and Pezeshk (1999)). 5% damped response spectra can then be derived from these recordings, both for a reference rock profile and by subsequently applying the corresponding predicted Fourier amplification function of the particular site. The ratio between the response spectrum on sediments and that on the reference rock was then calculated to obtain the final amplification function in terms of response spectral ordinates. Since we deal with anelastic amplification functions, the spectra of the reference rock were adjusted for the attenuation (*Kappa0*; Anderson and Hough, 1984) of the Japanese reference profile. This reference profile and the value of 0.023s for *Kappa0* have been established in a previous study (Poggi et al., 2013).

3 - Site selection and input parameters

For the comparison in our study, a subset of 88 (out of a total of 660) stations of the Japanese KiKNet strong-motion network (Aoi et al., 2004) was used. The selection was driven by the requirements of the AUTH classification scheme, whose site classes were available only for a subset of KiKNet stations (Table 1, Figure 1, Figure 2 top) in southern Japan. For each test site, Vs30 values were computed as the travel-time average from the S-wave velocity profiles made available by the Japanese National Research Institute for Earth Science and Disaster Prevention (NIED), as obtained from downhole seismic logging. The selection covers a wide range of Vs30 values between 100 and 800m/s, with the larger number of sites in the interval 300-400m/s (Figure 2 bottom). PGA values were obtained from 37382 recordings spanning a wide range of magnitude and distance combinations. PGA is well represented in the range 0.001-1 m/s^2 (Figure 3); values above and below were discarded from the analysis in order to focus on ground-motions of engineering interest, whilst avoiding strong non-linear soil behavior, which is not considered in this study.

For the stochastic modeling, we produced a large set of response spectra covering a representative combination of magnitude, distance and stress-drop values as listed in Table 2. We noted relatively limited impact of the choice of individual parameter combinations due to the fact that a ratio is taken between amplified site-specific spectra and reference spectra with identical input parameters for the source and path. For the comparison with AUTH and METU results, all response spectral amplification functions obtained from these input parameter combinations were averaged (in the log-space) to produce mean site-specific models.

4 - Adjusting for a common reference

The AUTH and METU response spectral amplification functions are referenced to a common rock condition, which was defined within the SHARE project as a piece-wise gradient-like velocity profile with Vs30 (travel-time average shear-wave velocity in the

upper 30m) of 800m/s (see Boore and Joyner, 1997). This reference is different to that used in the SED model (Figure 4), which was directly calibrated to the rather different rock conditions of Japan (Poggi et al., 2013). The SED Japanese reference profile consists of a gradient with a steep increase in velocity in the first 300m, from about 1100m/s to almost 3000m/s. The Vs30 of this reference is about 1350m/s, which identifies the profile as a hard-rock reference in standard Vs30-based classification schemes (e.g. NEHRP, Building Seismic Safety Council, 2003). A more exhaustive description of how this reference has been retrieved can be found in Poggi et al. (2013).

To adjust the SED stochastic amplification model to the SHARE reference conditions, we make use of a procedure based on the quarter-wavelength method as described in Edwards et al. (2013). According to this approach, the SED Fourier amplification functions $A_{SH}(f)$ has to be multiplied by a frequency-dependent correction function $C(f)$ (Figure 5) to compensate for the different reference conditions:

$$A_{SH}^{Corr}(f) = C(f)A_{SH}^{Base}(f). \qquad \text{Eq. 1}$$

where $C(f)$ is a function of the quarter-wavelength average-velocities of both the local (SED) and the target (SHARE) reference profiles:

$$C(f) = \sqrt{\frac{\overline{Vs}_{Target}^{Qwl}(f)}{\overline{Vs}_{Local}^{Qwl}(f)}}. \qquad \text{Eq. 2}$$

It can be noticed that the SHARE rock profile has much lower velocities close to the surface with respect to the Japanese reference. The correction function leads therefore to a general reduction of the amplification level over the analyzed frequency bands (Figure **6**). This is also evident by comparing the amplification functions of the two reference rock profiles (Figure 5) with respect to the common basement reference (a half-space with Vs of ~3000m/s).

From the adjusted Fourier amplification models, response spectral amplification functions are then derived by means of the random vibration theory approach (Boore, 2003).

5 - Site classes

In this study the comparison between the different response spectral amplification functions is performed for different soil conditions separately. We used two different approaches to discriminate soil types; a Vs30 approach and a soil classification scheme. For the Vs30 based approach, it was decided to split the available 88 sites into 5 classes, ranging from 200m/s to 700m/s with a 100m/s interval. An additional class for those remaining sites with Vs30 > 700m/s is also used to represent rock conditions. Complementary to this approach, for the soil type classification we used the AUTH classification scheme. For each of the 88 selected stations, bedrock depth (Z) was first evaluated by AUTH using the available borehole logs from the KiKNet database and the average velocity (VsZ) calculated, while f_0 of the sites was empirically determined form horizontal to vertical Fourier spectral ratios (H/V) of earthquake recordings. However, using such approach, some subclasses were not sufficiently populated to produce usable statistics. Therefore, some grouping of the AUTH classes was necessary (B1+B2 and C1+C2+C3). Moreover, class D was not represented in the original selection of 88 sites, and is therefore disregarded from the analysis.

6 - Comparing amplification functions

6.1 - Average of all sites

Firstly, we compared response spectral amplification functions from the AUTH, METU and SED models for all the available 88 sites (e.g. Figure 7) and then computed the mean of the log-residual distribution (Figure 8). We note that residual refers to the difference between models only, and does not imply any comparison with data. The comparison was performed both with and without adjustment for the common reference

9

(Figure 9). This was useful to highlight the general impact on ground motion amplification of using a homogeneous reference, which results in a positive offset of the residual functions, while keeping nevertheless the main features of the amplification models (e.g. resonance peaks and troughs) substantially unmodified.

The comparison between AUTH and METU results showed good agreement (Figure 8a). Although the mean of the log-residual distribution is slightly - but consistently - shifted to positive values (the AUTH model predicts stronger amplification), the data scatter is quite small over the whole frequency range of the comparison (0.5-100Hz). This is partially due to the fact that the two approaches were based on the same dataset, but it can also be explained by the simplified shapes of the used amplification functions, which can only partially account for local phenomena like resonance and anelastic attenuation.

On the contrary, SED predictions are strongly site-dependent, as they are based on the whole local velocity profile, with strong influence from the particular velocity interfaces at shallow depths. The velocity contrasts are the main source of resonance effects. Moreover, the coefficients of the SED prediction equation are implicitly calibrated using the site *Kappa0* operators. By comparing SED functions with the AUTH (Figure 8b) and METU (Figure 8c) results, therefore, larger deviations can be observed on average, in particular at intermediate frequencies - at around 5Hz - where the average effect of resonance in soft sediment site is more pronounced, and the SED model predicts the larger site-specific amplifications. The scatter of the residual distribution is also generally higher over the whole analyzed frequency range due to the highly site-specific nature of the SED computations. In **Figure 9**, the broadband offset is removed from the amplification function difference, which is always negative, meaning that for the reference rock condition (Vs30 of 800 m/s) AUTH and METU predict higher ground motions than the adjusted SED model.

6.2 - Analysis for the site classes

In a second step, the analysis was performed on sub-selections of sites based on Vs30 and soil type classification as previously introduced. In this case, a wider spectrum of variability of the log-residual curves was found. In more detail, comparing the AUTH and METU results shows a moderate positive offset of the residual functions (Figure 10); this implies higher values of the AUTH amplification model with respect to METU, on average. Differences are more evident at the edges of the soil class spectrum, and particularly for very stiff soil/rock conditions (Vs30 > 700m/s).

These differences, other than to the different approaches used for the analyses, might be addressed to some bias in the selection of the sites used for the calibration of the two models. Reliable information about the velocity structure beneath a seismic station is not always available, and therefore Vs30 is often extrapolated by indirect methods, e.g. by geological/geotechnical classification of the surface deposits. Such an approach, however, might introduce large uncertainties in the metadata of the calibration dataset, which can then affect the stability of the resulting amplification functions.

On the other hand, the SED response amplification model shows more significant deviations in comparison to the two SHARE models (Figure 11 and Figure 12). In this case, dependency on the soil type is more evident. A lower amplification of the SED model for stiff material is observed when compared to the SHARE models, while a higher amplification is modeled the softer the sediments. Particularly interesting is to observe how the trough (minimum) of the amplification-difference plots moves between the different curves from low frequency (about 3Hz) in loose material, to high frequency (about 10Hz) in rock-like sites. This is clear confirmation that such minimum should be related to presence of site-specific resonance effects, which are (to a certain extent) accounted for in the SED model, but not in the SHARE models.

Anelasticity has a significant effect on SED Fourier amplification models (as seen in Figure 6). In terms of response spectral amplification, this effect is less substantial due

to the reduced sensitivity of high oscillator-frequency earthquake response spectra to the same driving (i.e. FAS, Fourier Amplitude Spectra) frequencies (Bora et al., 2016). The result is typically seen as a minimum in the SED response spectral amplification functions, leading to a peak in the amplification-difference plots. Evaluating the impact of anelasticity on the distribution of the response spectral amplification residuals is therefore not straightforward. Most likely, the positive peak at about 20Hz in the residual difference plots (Figure 11 and Figure 12), which is rather stable and present in all the curves, can be related to the amplitude decay (due to local attenuation) in the SED amplification model. From this observation, it appears that the SHARE models may not fully account for the effect of attenuation at high frequencies, a point that should be further investigated.

The reader can find the actual amplification factors (in linear scale) also presented in Table 3, Table 4 and Table 5 for a selected number of frequencies.

7 - Summary and conclusions

The comparison between 5% damped response spectral amplification functions from AUTH, METU and SED provides useful insights about the present level of epistemic uncertainty in site-response modeling using empirical approaches. It is presently not possible (and it is certainly not the scope of this study) to define which one of the three methods is the most suitable or the best performing in general, because each of the tested approaches was implemented following a different strategy and according to different requirements in terms of input and output constraints. In fact, for the same reason, we tried to avoid any direct comparison between modeled and observed amplification functions. It is nevertheless possible to summarize few important considerations out of the performed analysis.

First, it is important to understand the source of the variability between methods. As we observed, the largest differences are seen in those frequency bands where resonance phenomena and effect of anelastic attenuation are statistically more relevant. The SED

approach is more likely to explain the occurrence of these phenomena, using more input information required for the modeling (the entire velocity profile and site-specific *Kappa0,* and not only Vs30). On the other hand, the METU model is less demanding in terms of site information (only Vs30 is required, aside from PGA to quantify non-linearity level), but appears to not adequately represent the occurrence of the aforementioned resonance phenomena and is instead averaging across a wide variety of sites. AUTH's approach is potentially a good compromise between type and amount of input calibration parameters (average velocity VsZ and fundamental frequency of resonance f_0) and model complexity. However, the use of simplified design spectral shapes tends to significantly smear the site-specific information as well, losing the benefit of accounting for site-resonance. Moreover, the SHARE models might be affected by the assumptions and metadata used to derive the models. With the observations in **Figure 9**, we might argue that the ground motion at reference rock-condition of Vs30 of 800m/s is affected by softer sites used to derive the model. Presently, this is simply a speculation that might be proven once the quality of the metadata improves in the future.

What is currently missing in this study, and that is certainly the target of a follow-up analysis, is the evaluation of the impact of uncertainty from the site parameters, and the dependence of the results on magnitude and distance. It is a well-known fact that most site proxies, particularly the Vs30, are often poorly determined at single sites and will improve in the future due to efforts at national level (e.g. Michel et al., 2014). For large-scale mapping, furthermore, these proxies are often derived from other proxies such as topographic slope (Wald and Allen, 2007) shown to be unreliable for site-specific studies (Lemoine et al., 2012). Although the effect of uncertainty of site proxies on the derived amplification can easily be guessed, a rigorous quantification, or even better the modeling of this effect is still missing in many applications.
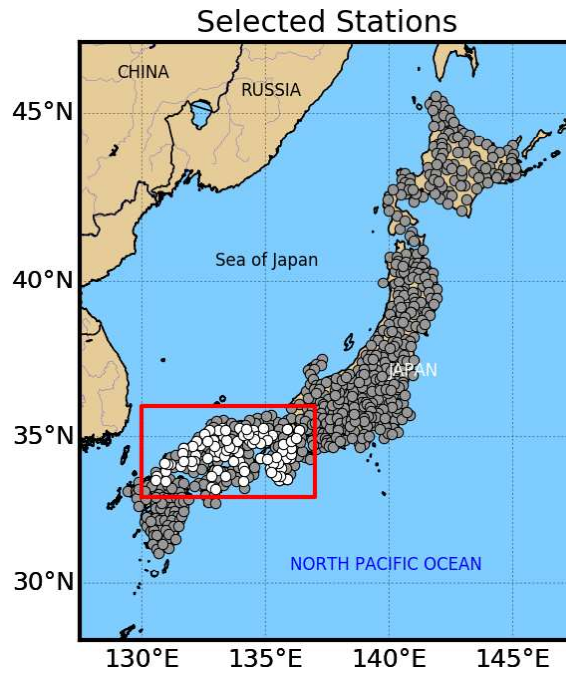
8 - Acknowledgments

References

Abrahamson, N.A., Silva, W.J., 2008. Summary of the Abrahamson & Silva NGA ground motion relations, *Earthquake Spectra.* 24, 67-97.

Anderson, J.G., Hough S.E., 1984. A model for the shape of the Fourier amplitude spectrum of acceleration at high-frequencies, *Bull. Seismol. Soc. Am.* 74, 1969-1993.

Aki, K., 1988. Local site effects on strong ground motion. *Earthquake Engineering and Soil Dynamics II - Recent Advances in Ground Motion Evaluation.* June 27-30, Park City, Utah.

Aoi, S., Kunugi, T., Fujiwara H., 2004. Strong-motion seismograph network operated by NIED: K-Net and KiK-Net, *J. Japan Assoc. Earthq. Eng.* 4, 65-74.

Boore, D.M., Joyner, B., 1997, Site amplifications for generic rock sites, *Bull. Seismol. Soc. Am.*, 87, 2, 327-341.

Boore, D.M., 2003. Simulation of ground motion using the stochastic method, *Pure and Applied Geophysics*, 160, 635-676.

Bora, S.S., Scherbaum, F., Kuehn, N., Stafford, P., 2016. On the Relationship between Fourier and Response Spectra: Implications for the Adjustment of Empirical Ground-Motion Prediction Equations (GMPEs). *Bull. Seismol. Soc. Am*, 106, 3, 1235-1253.

Building Seismic Safety Council, 2003. The 2003 NEHRP recommended provisions for new buildings and other structures, Part 1: Provisions (FEMA 450), www.bssconline.org (last accessed February 2016).

Cartwright, D.E., Longuet-Higgins, M.S., 1956. The Statistical distribution of the maxima of a random function, *Proceedings of the Royal Society of London Series a-Mathematical and Physical Sciences.* 237, 212-232.

Cotton, F., Scherbaum, F., Bommer, J.J., Bungum, H., 2006. Criteria for selecting and adjusting ground-motion models for specific target regions: Application to Central Europe and rock sites. *J. Seism.* 10, 137-156.

CEN, European Committee for Standardization, 2004. Eurocode 8: design of structures for earthquake resistance-part 1: general rules, seismic actions and rules for buildings. Bruxelles.

Douglas, J., Edwards, B., 2016. Recent and Future Developments in Earthquake Ground Motion Estimation, Earth-Science Reviews, doi: http://dx.doi.org/10.1016/j.earscirev.2016.07.005.

Edwards, B., Poggi, V., Fäh, D., 2011. A Predictive equation for the vertical-to-horizontal ratio of ground motion at rock sites based on shear-wave velocity profiles from Japan and Switzerland, *Bull. Seismol. Soc. Am.* 101, 6, 2998-3019.

Edwards B., Michel C., Poggi V., Fäh D., 2013, Determination of site amplification from regional seismicity: application to the Swiss national seismic networks, *Seismological Research Letters*. 84, 4, 611-621.

Faccioli, E., 1991. Seismic amplification in the presence of geological and topographic irregularities, *Proceedings of the Second International Conference on Recent Advances in Geotechnical Earthquake Engineering and Soil Dynamics*, March 11-15, St. Louis, Missouri, 2, 1779-1797.

Joyner, W.B., Warrick, R.E., Fumal, T.E., 1981. The effect of Quaternary alluvium on strong ground motion in the Coyote Lake, California, earthquake of 1979, *Bull. Seismol. Soc. Am.* 71, 4, 1333-1349.

Lemoine, A., Douglas, J., Cotton, F., 2012. Testing the applicability of correlations between topographic slope and Vs30 for Europe. - *Bull. Seismol. Soc. Am*. 102, 6, 2585-2599.

Liu, L., Pezeshk, S., 1999. An Improvement on the estimation of pseudoresponse spectral velocity using rvt method, *Bull. Seismol. Soc. Am.* 89, 1384-1389.

Michel, C., Edwards, B., Poggi, V., Burjanek, J., Roten, D., Cauzzi, C., Fäh, D., 2014. Assessment of site effects in alpine regions through systematic site characterization of seismic stations, *Bull. Seismol. Soc. Am.* 104, 6, 2809-2826.

Pitilakis, K., 2004. Site effects. In *Recent Advances in Earthquake Geotechnical Engineering and Microzonation*, Springer Netherlands, 139-197.

Pitilakis K, Anastasiadis A, Riga, E., 2012 New site classification scheme and associated site amplification factors. SHARE Deliverable 4.3.

Poggi, V., Edwards, B., Fäh, D., 2011. Derivation of a reference shear-wave velocity model from empirical site amplification, *Bull. Seismol. Soc. Am.* 101, 1, 258-274.

Poggi, V., Edwards, B., Fäh, D., 2012a. The quarter-wavelength average velocity: a review of some past and recent application developments. *Proceedings of the 15th WCEE*. Lisbon, Portugal.

Poggi, V., Edwards, B., Fäh, D., 2012b. Characterizing the vertical to horizontal ratio of ground-motion at soft sediment sites, *Bull. Seim. Soc. Am.*, 102, 6, 2741-2756.
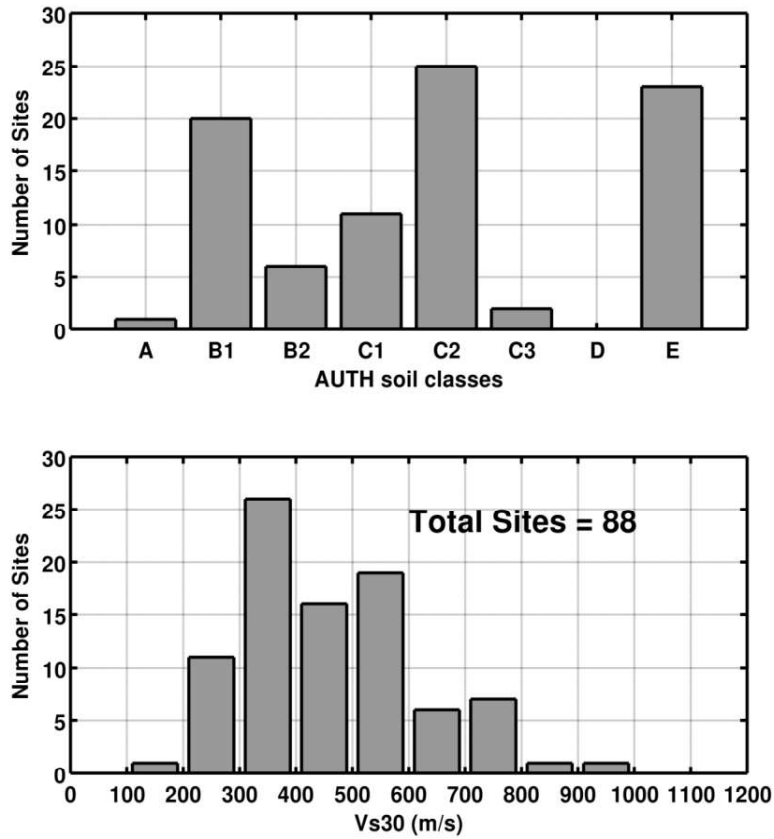
Poggi, V., Edwards, B., Fäh, D., 2013. Reference S-wave velocity profile and attenuation models for ground-motion prediction equations: application to Japan, *Bull. Seim. Soc. Am.*, 103, 5, 2645-2656.

Sandıkkaya, M.A., Akkar, S., Bard, P.-Y., 2013. A nonlinear site-amplification model for the next pan-european ground-motion prediction equations. *Bull. Seismol. Soc. Am.*, 103, 1, 19–32.

Van Houtte, C., Drouet, S., Cotton, F., 2011. Analysis of the origins of κ (kappa) to compute hard rock to rock adjustment factors for GMPEs. *Bull. Seismol. Soc. Am.* 101, 6, 2926-2941.

Wald, D.J., Allen, T.I., 2007. Topographic slope as a proxy for seismic site conditions and amplification, *Bull. Seism. Soc. Am*, 97, 5, 1379-1395.

Wells, D.L., Coppersmith, K.J., 1994. New empirical relationships among magnitude, rupture length, rupture width, rupture area, and surface displacement, *Bull. Seismol. Soc. Am.* 84, 974-1002.

Woessner, J., Laurentiu, D., Giardini, D., Crowley, H., Cotton, F., Grünthal, G., Valensise, G., Arvidsson, R., Basili, R., Demircioglu, M.B., Hiemer, S., Meletti, C., Musson, R.W., Rovida, A.N., Sesetyan, K., Stucchi, M., 2015. The 2013 European Seismic Hazard Model: key components and results. *Bull. Earth. Eng.*, 13, 12, 3553-3596.

FIGURES
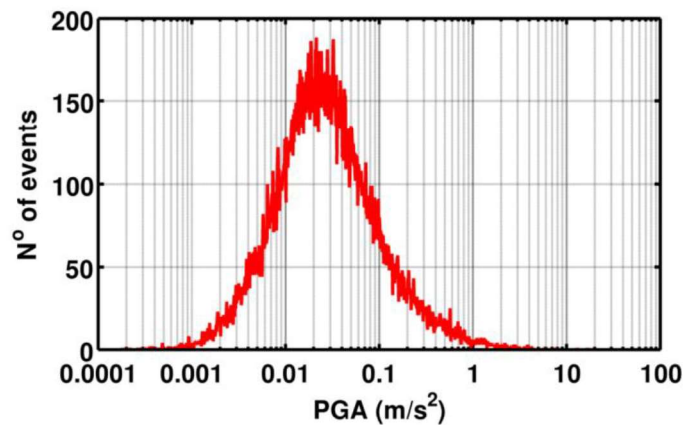

Figure 1. *Location of the 88 selected testing sites (white circles) of the Japanese KiKNet strong-motion network (gray circles).*

Figure 2. *Distribution of the AUTH soil classes (on top) and Vs30 values (bottom) for the 88 selected sites of the Japanese KiKNet strong-motion network. Note that class D was not excluded, but is not represented in the selection.*

Figure 3. *Distribution of the 37382 PGA values available for the 88 selected sites of the Japanese KiKNet strong-motion network.*

19
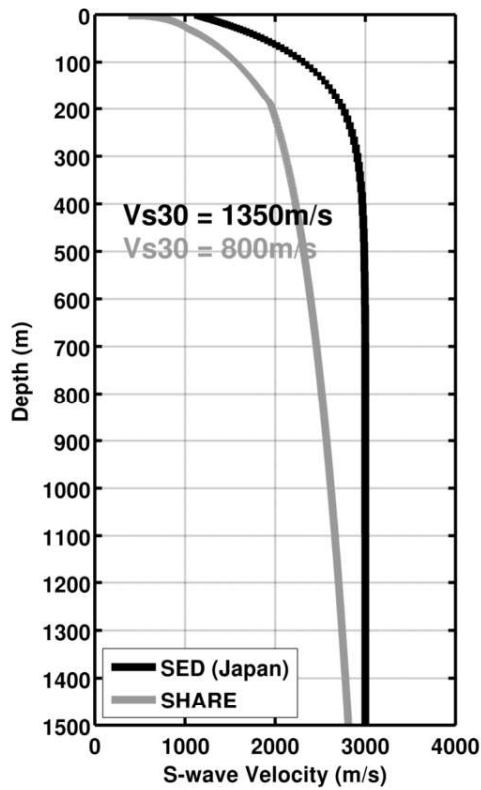
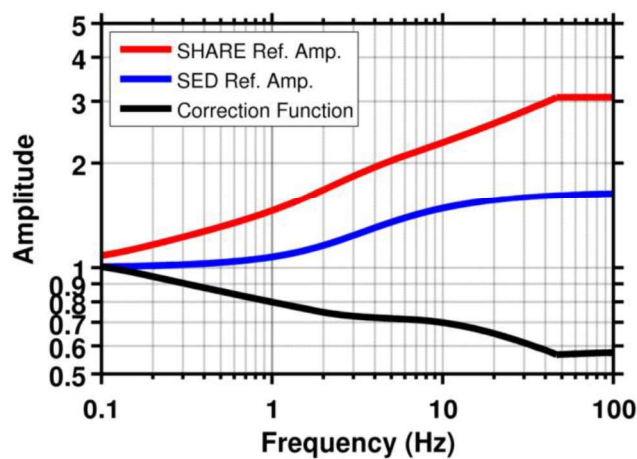**Figure 4.** *Comparison between the SHARE (in gray) and SED (in black) Japanese rock reference S-wave velocity profiles.*
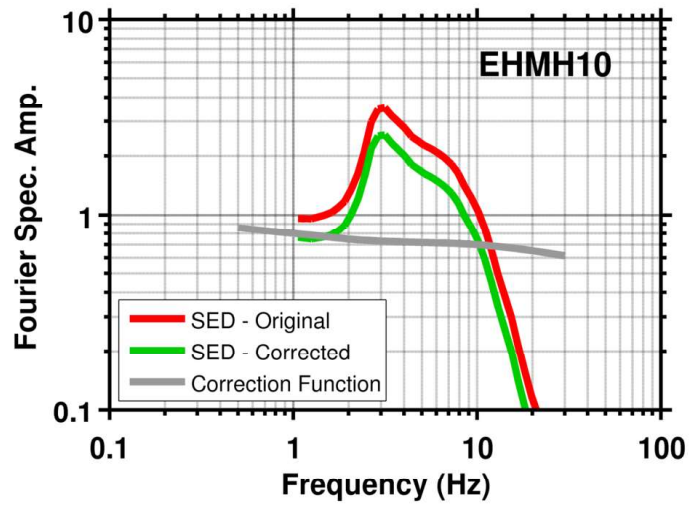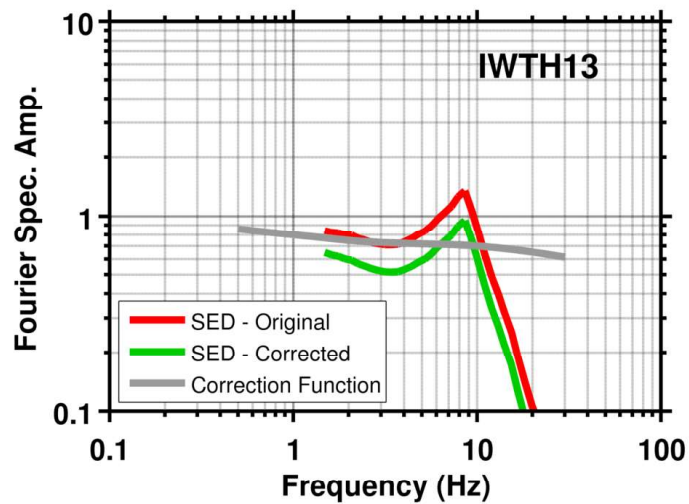

Figure 5. *The correction function C(f) (in black) in comparison with the quarter-wavelength amplification functions of the SED Japanese (in blue) and SHARE (in red) references.*

20

A) Vs30 = 318m/s

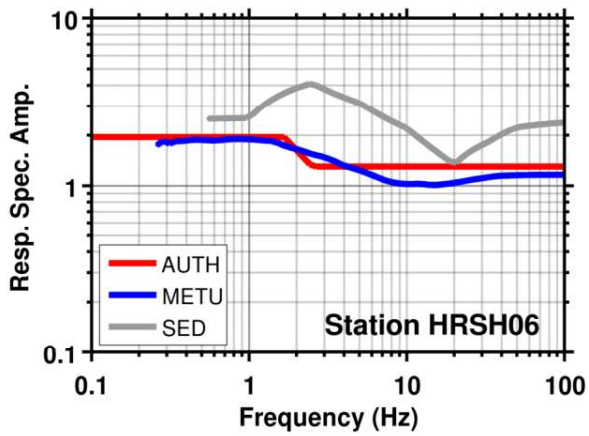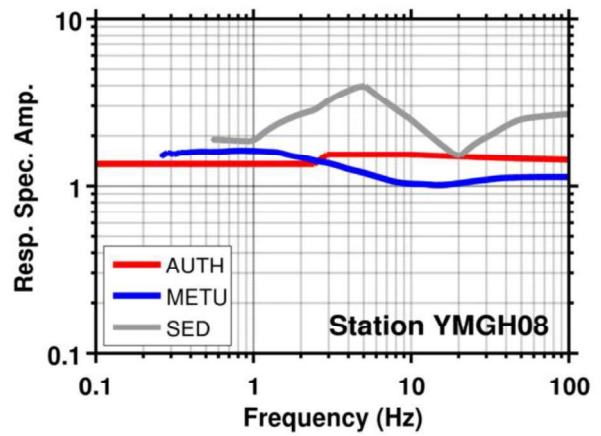B) Vs30 = 620m/s

Figure 6. *Example of Fourier spectral amplification functions at two stations of the Japanese KiK-Net network, before (in red) and after (in green) the correction for the SHARE reference. The correction results in a general decrease in the amplification level over the whole frequency band.*

A) Vs30 = 279m/s, Class C2

D) Vs30 = 342m/s, Class E

E) Vs30 = 440m/s, Class C1
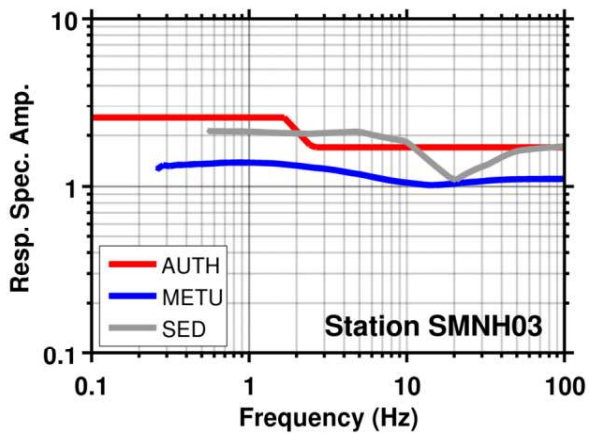
B) Vs30 = 504m/s, Class E
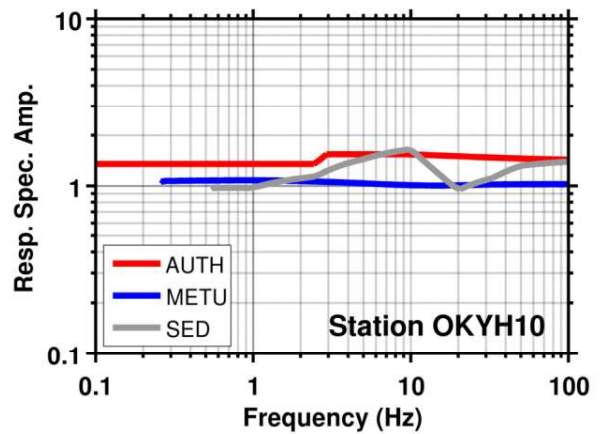
C) Vs30 = 940m/s, Class B1
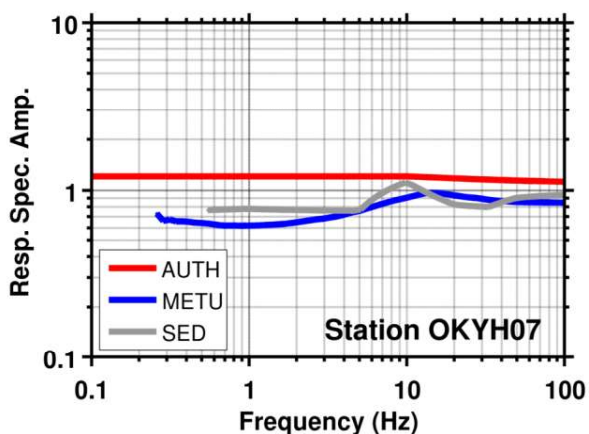
F) Vs30 = 1387m/s, Class A
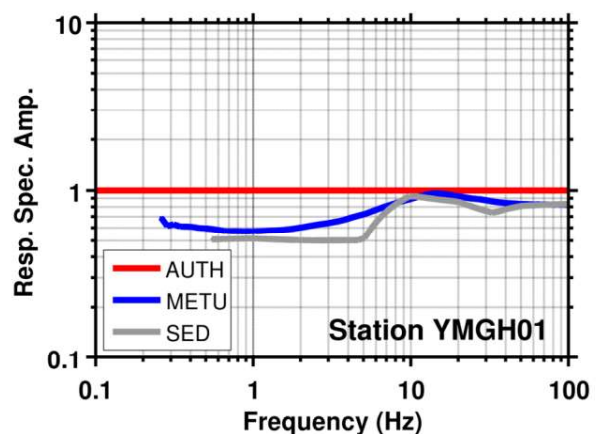
Figure 7. *Examples of comparison between AUTH, METU and SED response spectral amplification at sites of different characteristics (Vs30 and soil class as in Table 1).*
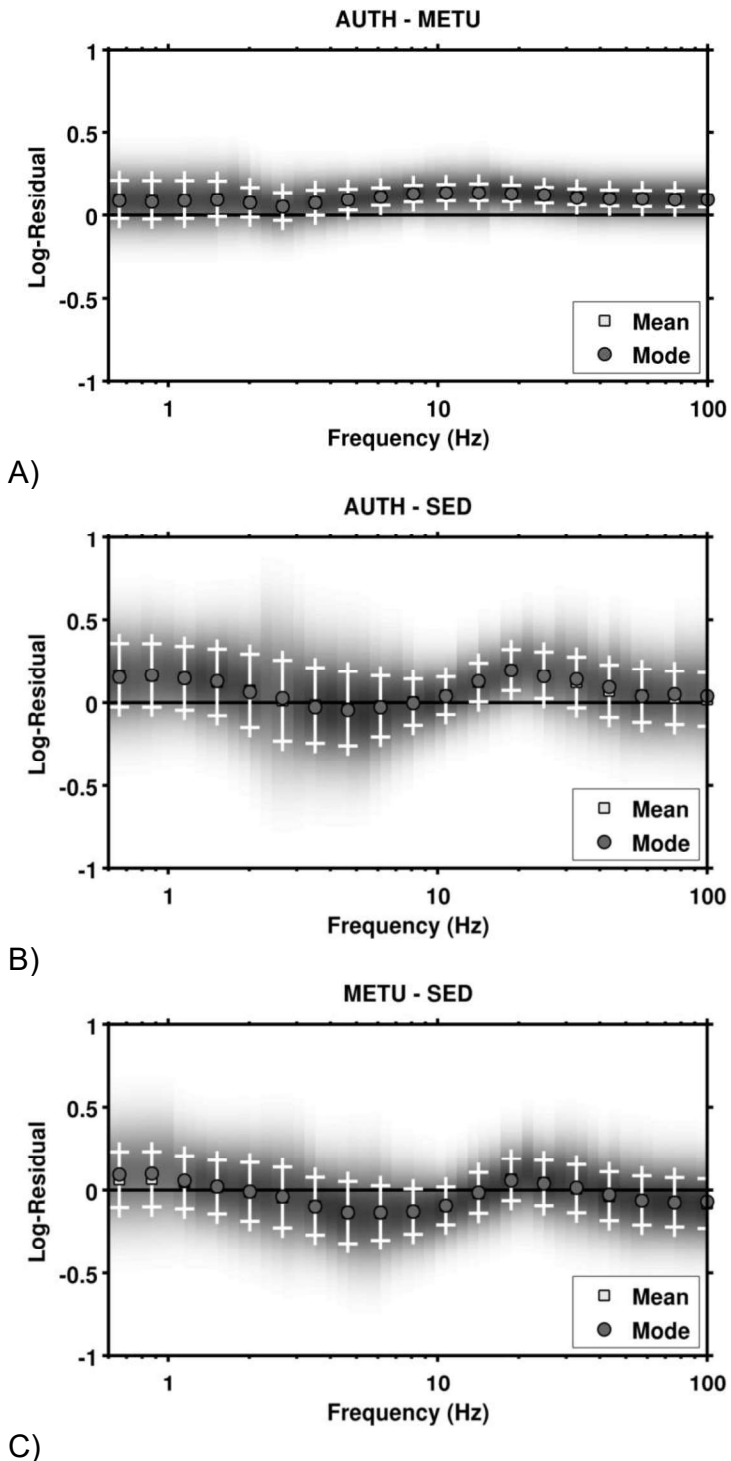
Figure 8. *Distribution of log-residuals (base 10) of the three comparisons between response spectral amplification functions from METU, AUTH and SED in the frequency range 0.5-100Hz (white error bars show mean +/- standard deviation). The three analyzed models are here referred to the same common reference. All 88 selected sites are used for the statistic.*
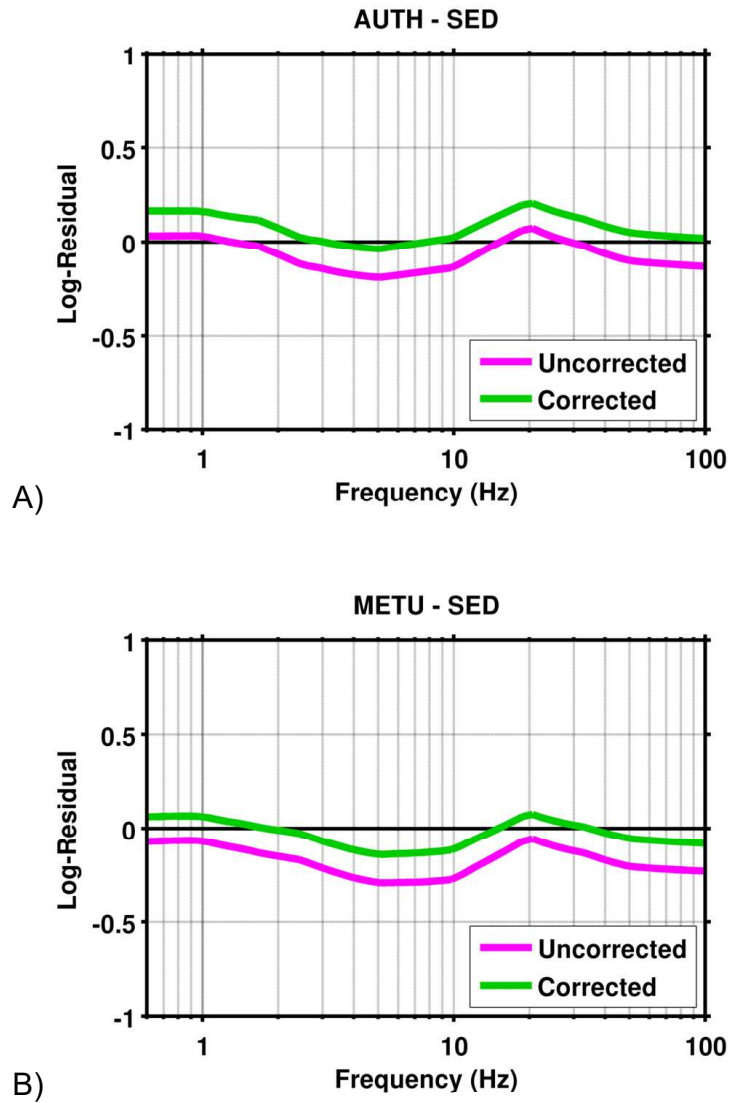
Figure 9. *Comparison between the SED-AUTH and SED-METU log-residual mean (base 10) without (in magenta) and with (in green) the adjustment for the common SHARE reference. From the picture the effect of the reference correction on the analysis is clear.*
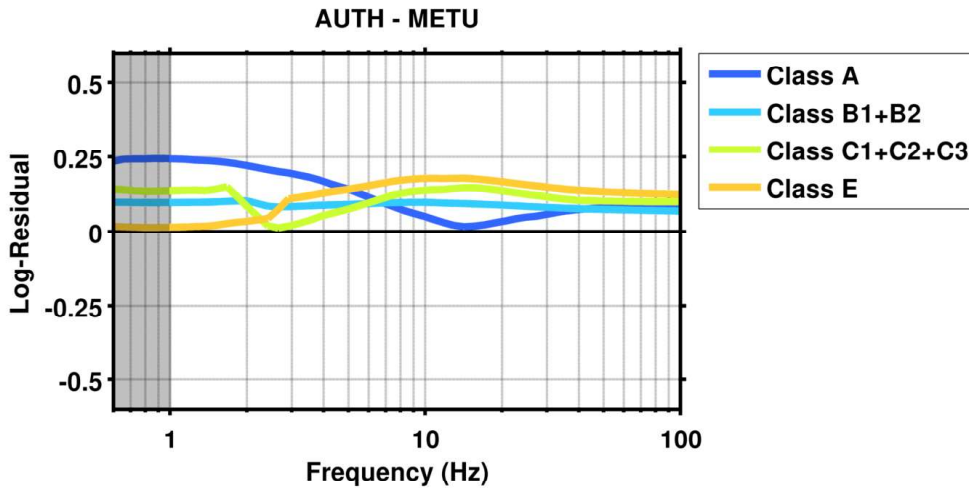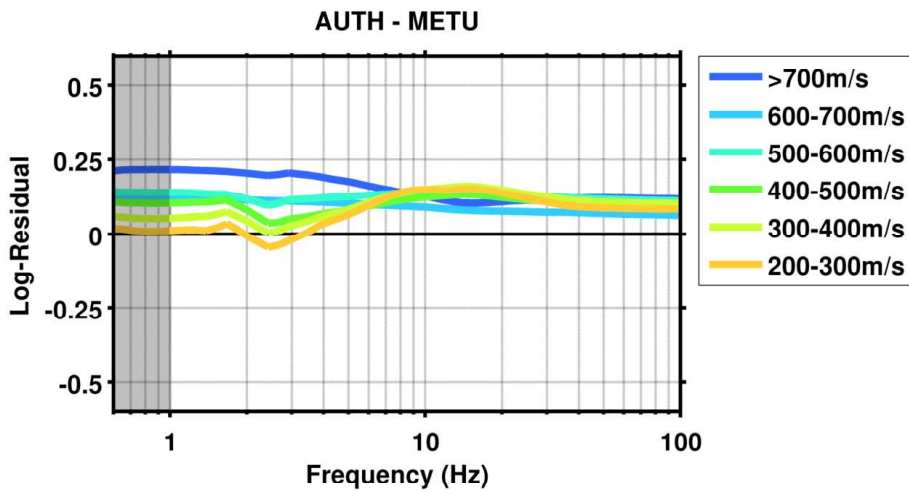
Figure 10. *Variability on the average log-difference between AUTH and METU models with respect to different soil classes (A) and Vs30 ranges (B). The gray area below 1Hz indicates the region where the statistic might be biased by lack of sufficient data points.*

Figure 11. *Variability on the average log-difference between AUTH and SED models with respect to different soil classes (A) and Vs30 ranges (B). The gray area below 1Hz indicates the region where the statistic might be biased by lack of sufficient data points.*

26

A)

B)

Figure 12. *Variability on the average log-difference between METU and SED models with respect to different soil classes (A) and Vs30 ranges (B). The gray area below 1Hz indicates the region where the statistic might be biased by lack of sufficient data points.*

TABLES

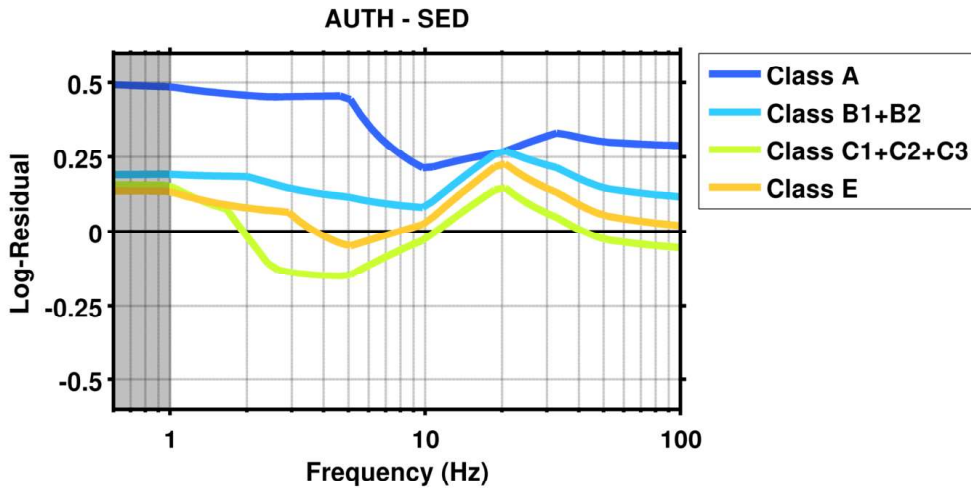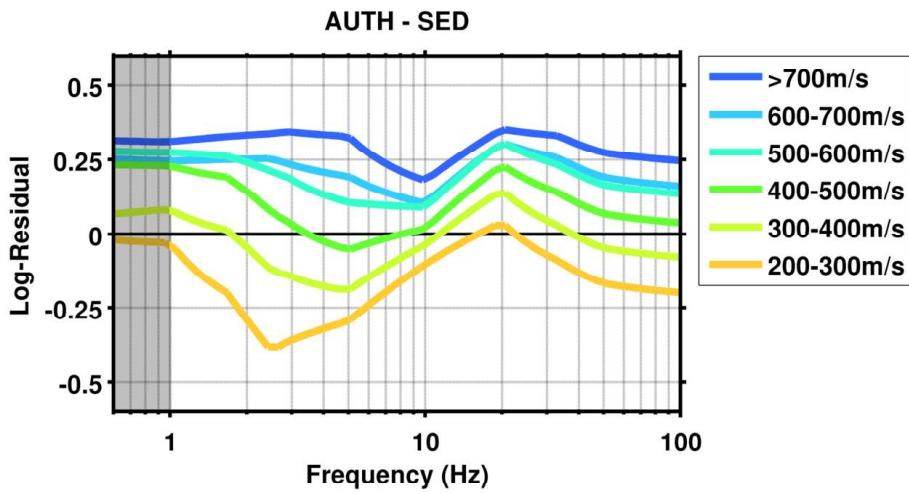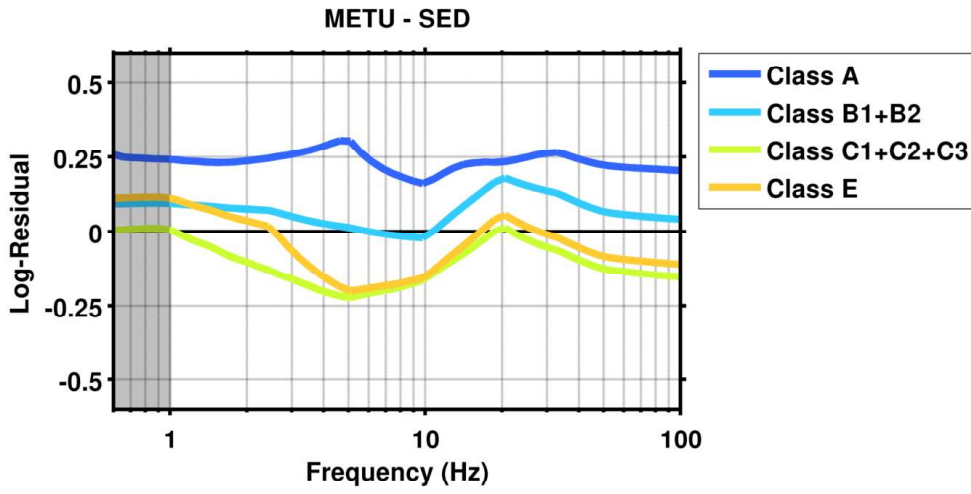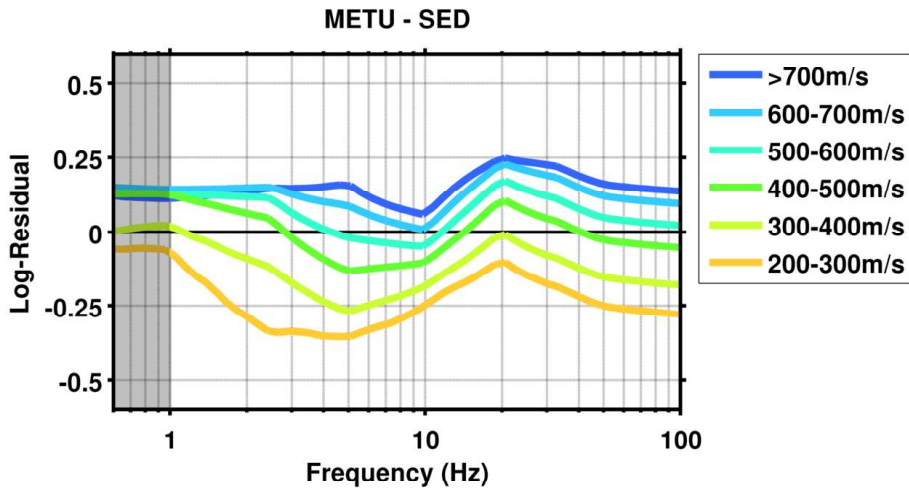| ID	Vs_{30}	Class	ID	Vs_{30}	Class	ID	Vs_{30}	Class	ID	Vs_{30}	Class
EHMH04	260	C1	HYGH06	369	C2	OKYH05	620	B1	TTRH01	437	B1
EHMH05	364	C2	HYGH07	506	B1	OKYH06	555	B2	TTRH02	310	C1
EHMH06	717	B1	HYGH08	288	E	OKYH07	940	B1	WKYH01	463	E
FKOH01	588	E	HYGH09	365	B2	OKYH08	694	B1	WKYH02	369	E
FKOH02	273	C2	HYGH10	224	C3	OKYH10	504	E	WKYH03	547	E
FKOH03	504	B1	HYGH11	271	C2	OKYH11	543	B1	WKYH04	550	E
FKOH05	777	E	HYGH12	677	B1	OKYH12	757	B1	WKYH05	591	C3
HRSH01	403	C2	KGWH01	255	C2	OSKH03	408	C2	WKYH06	756	E
HRSH02	391	E	KGWH02	185	C2	OSKH04	529	B1	WKYH07	316	C2
HRSH03	487	C2	KOCH01	363	C2	SIGH01	563	E	WKYH08	344	C1
HRSH04	458	E	KOCH02	394	E	SIGH02	569	E	WKYH09	349	C1
HRSH05	382	B2	KOCH03	677	B1	SIGH03	393	B2	WKYH10	466	C2
HRSH06	279	C2	NARH01	338	C2	SIGH04	483	B2	YMGH01	1387	A
HRSH07	462	B2	NARH03	497	E	SMNH01	464	C2	YMGH02	398	C2
HRSH08	781	B1	NARH04	592	B1	SMNH02	510	C1	YMGH03	536	B1
HRSH09	496	B1	NARH05	398	E	SMNH03	440	C1	YMGH04	659	B1
HRSH10	265	C2	NARH06	370	E	SMNH04	285	E	YMGH05	450	C2
HYGH01	344	C1	NIGH11	375	C1	SMNH05	711	B1	YMGH07	351	C2
HYGH02	612	B1	NIGH12	553	C1	SMNH06	293	C1	YMGH08	342	E
HYGH03	528	C2	OKYH01	238	C2	SMNH07	318	C1	YMGH09	304	C2
HYGH04	476	C2	OKYH03	317	C2	TKSH02	349	E	YMGH10	526	C2
HYGH05	533	E	OKYH04	360	E	TKSH03	404	E	YMGH11	711	B1

Table 1. *List of the 88 target stations of the Japanese KiKNet strong-motion network for which AUTH soil classes were available.*

Parameter	Range
Magnitude (M_w)	4, 5, 6
Joyner-Boore Distance (R_{JB})	10, 20, 30, 50 Km
Hypocentral Depth (D)	12 Km
Fault Model	Wells and Coppersmith (1994) Strike-Slip with 79 degree dip
Attenuation Model	Edwards et al. (2011)
Stress drop ($\Delta\sigma$)	60, 90, 120 bars

Table 2. *Ranges of the parameters used for the stochastic modeling of response spectra.*

AUTH/METU - Class Selection

Freq. (Hz)	1	1.27	1.62	2.07	2.64	3.36	4.28	5.46	6.95	8.86	11.29	14.38	18.33	23.36	29.76	48.33	100
A	1.75	1.73	1.71	1.65	1.59	1.53	1.44	1.35	1.24	1.16	1.09	1.04	1.07	1.11	1.14	1.2	1.22
B1+B2	1.25	1.25	1.26	1.26	1.21	1.22	1.23	1.24	1.25	1.25	1.25	1.24	1.23	1.22	1.21	1.19	1.17
C1+C2+C3	1.37	1.38	1.41	1.18	1.03	1.08	1.15	1.22	1.3	1.36	1.38	1.4	1.38	1.34	1.31	1.27	1.26
E	1.03	1.04	1.06	1.09	1.18	1.31	1.36	1.4	1.46	1.5	1.51	1.51	1.48	1.44	1.41	1.36	1.33

AUTH/METU - Velocity Selection

Freq. (Hz)	1	1.27	1.62	2.07	2.64	3.36	4.28	5.46	6.95	8.86	11.29	14.38	18.33	23.36	29.76	48.33	100
>700m/s	1.64	1.64	1.62	1.59	1.58	1.58	1.53	1.48	1.41	1.36	1.31	1.27	1.27	1.29	1.3	1.32	1.31
600-700m/s	1.31	1.3	1.3	1.3	1.29	1.28	1.27	1.26	1.25	1.23	1.22	1.2	1.19	1.19	1.18	1.17	1.15
500-600m/s	1.38	1.37	1.36	1.3	1.26	1.31	1.32	1.34	1.36	1.38	1.38	1.38	1.37	1.35	1.33	1.31	1.29
400-500m/s	1.27	1.27	1.29	1.18	1.09	1.14	1.18	1.22	1.27	1.31	1.34	1.35	1.33	1.31	1.28	1.25	1.23
300-400m/s	1.13	1.14	1.18	1.09	1.02	1.09	1.17	1.24	1.32	1.39	1.42	1.45	1.42	1.37	1.33	1.28	1.26
200-300m/s	1.03	1.03	1.07	0.97	0.91	1	1.11	1.2	1.32	1.4	1.4	1.41	1.39	1.33	1.28	1.22	1.21

Table 3. *AUTH versus METU average response spectral amplification factors.*

AUTH/SED - Class Selection

Freq. (Hz)	1	1.27	1.62	2.07	2.64	3.36	4.28	5.46	6.95	8.86	11.29	14.38	18.33	23.36	29.76	48.33	100
A	3.05	2.97	2.91	2.86	2.83	2.84	2.85	2.54	2	1.71	1.66	1.75	1.82	1.94	2.09	2.01	1.95
B1+B2	1.55	1.54	1.53	1.52	1.43	1.37	1.32	1.28	1.24	1.21	1.31	1.54	1.79	1.79	1.67	1.42	1.31
C1+C2+C3	1.41	1.29	1.2	0.93	0.74	0.72	0.71	0.73	0.82	0.9	1.02	1.18	1.36	1.3	1.16	0.95	0.88
E	1.36	1.29	1.23	1.2	1.17	1.06	0.94	0.91	0.97	1.03	1.16	1.38	1.62	1.57	1.4	1.15	1.05

AUTH/SED - Velocity Selection

Freq. (Hz)	1	1.27	1.62	2.07	2.64	3.36	4.28	5.46	6.95	8.86	11.29	14.38	18.33	23.36	29.76	48.33	100
>700m/s	2.05	2.09	2.13	2.16	2.19	2.19	2.15	2	1.73	1.57	1.63	1.88	2.15	2.21	2.16	1.9	1.76
600-700m/s	1.76	1.77	1.78	1.79	1.76	1.66	1.59	1.5	1.38	1.3	1.38	1.64	1.92	1.94	1.84	1.57	1.44
500-600m/s	1.88	1.86	1.83	1.72	1.59	1.44	1.33	1.27	1.25	1.23	1.35	1.62	1.92	1.91	1.76	1.48	1.36
400-500m/s	1.69	1.61	1.56	1.36	1.15	1.02	0.92	0.91	0.96	1.02	1.14	1.36	1.61	1.57	1.42	1.18	1.09
300-400m/s	1.19	1.1	1.04	0.88	0.74	0.69	0.66	0.68	0.77	0.87	1	1.16	1.33	1.26	1.11	0.91	0.83
200-300m/s	0.91	0.75	0.64	0.49	0.42	0.45	0.49	0.54	0.63	0.74	0.84	0.95	1.06	0.98	0.85	0.69	0.63

Table 4. *AUTH versus SED average response spectral amplification factors.*

METU/SED - Class Selection

Freq. (Hz)	1	1.27	1.62	2.07	2.64	3.36	4.28	5.46	6.95	8.86	11.29	14.38	18.33	23.36	29.76	48.33	100
A	1.74	1.72	1.7	1.73	1.78	1.85	1.98	1.89	1.61	1.48	1.53	1.68	1.71	1.75	1.83	1.68	1.6
B1+B2	1.24	1.22	1.2	1.19	1.16	1.1	1.05	1.02	0.98	0.96	1.04	1.23	1.44	1.45	1.37	1.18	1.1
C1+C2+C3	1.01	0.92	0.84	0.78	0.72	0.66	0.62	0.61	0.63	0.66	0.74	0.85	0.99	0.97	0.88	0.75	0.7
E	1.29	1.21	1.14	1.08	0.97	0.79	0.68	0.63	0.65	0.68	0.76	0.9	1.08	1.07	0.98	0.83	0.77

METU/SED - Velocity Selection

Freq. (Hz)	1	1.27	1.62	2.07	2.64	3.36	4.28	5.46	6.95	8.86	11.29	14.38	18.33	23.36	29.76	48.33	100
>700m/s	1.3	1.31	1.34	1.37	1.4	1.4	1.43	1.37	1.24	1.17	1.26	1.5	1.7	1.73	1.68	1.46	1.37
600-700m/s	1.39	1.39	1.4	1.41	1.39	1.3	1.25	1.18	1.1	1.04	1.12	1.36	1.61	1.63	1.55	1.33	1.24
500-600m/s	1.34	1.33	1.32	1.31	1.25	1.1	1	0.95	0.92	0.9	0.98	1.17	1.41	1.42	1.32	1.13	1.05
400-500m/s	1.33	1.26	1.2	1.15	1.05	0.89	0.78	0.74	0.76	0.78	0.86	1.01	1.21	1.21	1.11	0.95	0.89
300-400m/s	1.04	0.95	0.87	0.8	0.73	0.63	0.56	0.55	0.58	0.63	0.7	0.8	0.94	0.92	0.84	0.71	0.66
200-300m/s	0.85	0.71	0.59	0.51	0.46	0.46	0.44	0.45	0.49	0.53	0.61	0.68	0.77	0.74	0.67	0.57	0.53

Table 5. *METU versus SED average response spectral amplification factors.*